UNIVERSITI PUTRA MALAYSIA

SYNTHESIS AND CHARACTERISATION OF PbS/Fe3O4 CORE SHELL QUANTUM DOTS BY MICROWAVE METHOD AT DIFFERENT VOLUME OF Fe3O4

AMBOK ZULHELMI BIN AMBOK DALEK

SYNTHESIS AND CHARACTERISATION OF PbS/Fe_3O_4 CORE SHELL QUANTUM DOTS BY MICROWAVE METHOD AT DIFFERENT VOLUME OF Fe_3O_4

By

AMBOK ZULHELMI BIN AMBOK DALEK

Thesis Submitted to the Department of Physics, Universiti Putra Malaysia, in partial Fulfilment of the Requirements for the Degree of Bachelor of Science (Hons.) in Physics

January 2022

DEDICATION

I dedicate my dissertation work to my family, my supervisor and many friends especially my group lab member. A special feeling of gratitude to my loving parents, Ambok Dalek and Mariani whose always pray for my success. Your words of encouragement and push for tenacity made me feel stronger day by day to complete my degree.

I also dedicate this dissertation to my supervisor, Dr Mazliana Ahmad Kamarudin who have supported me throughout the process. I will always appreciate all she has done, especially her time for helping me finishing my final year project and her knowledge that she shared with me.

I dedicate this work and give special thanks to my group lab member, Muhammad Fadil Bin Mohd Razali for being there for me throughout the semester. He helped me a lot inside and outside the lab. He also always having a discussion with me regarding on Quantum Dots. We both finally succeed our fyp and may success belong to you.

ABSTRACT

Synthesis and Characterization of PbS/Fe_3O_4 Core Shell Quantum Dots by Microwave Method at Different Volume of Fe_3O_4

by

Ambok Zulhelmi Bin Ambok Dalek

199146

January 2022

Supervisor: Dr. Mazliana Ahmad Kamarudin

Faculty: Faculty of Science

The synthesis of PbS/Fe_3O_4 core shell quantum dots with optimal synthesis parameters is analyzed by using photoluminescence (PL) and UV-Vis spectroscopy. The samples were prepared via microwave-assisted method. The optical properties effect on PL and UV-Vis's spectra is observed by changing the volume of Fe_3O_4 between 0.2, 0.4, and 0.6 ml. For the synthesis of PbS/Fe_3O_4 CSQDs, the temperature used was 55 °C, and the mixture was irradiated with microwave for 2 mins. The results have clearly indicated that the PbS/Fe_3O_4 allow shifting the optical features to higher emission energy as the volume of Fe_3O_4 increases. This blueshift in PL is understood as in the frame of migration of ion and exchange mechanism taking place during the synthesis. From the analysis of PL spectra, the energy band gap of PbS and PbS/Fe_3O_4 (0.2, 0.4, to 0.6 ml) was changed to 0.77, 2.67, 2.68, and 2.74 eV respectively. However, the analysis of energy band gap of PbS and PbS/Fe_3O_4 via UV-Vis was changed to 4.85,

3.61, 3.75, to 4.0 eV for PbS and PbS/Fe_3O_4 (0.2, 0.4, and 0.6 ml), respectively. This different of energy between PL and UV-Vis is due to Stoke shift occurs in the PbS/Fe_3O_4 CSQDs.

ABSTRAK

Sintesis dan Perincian Titik Kuantum Teras/Petala PbS/Fe_3O_4 dengan Kaedah Gelombang Mikro pada Isipadu Fe_3O_4 yang Berbeza

Oleh

Ambok Zulhelmi Bin Ambok Dalek

199146

Januari 2022

Penyelia: Dr. Mazliana Ahmad Kamarudin

Fakulti: Faculty Sains

Sintesis titik kuantum teras/petala PbS/Fe3O4 dengan parameter sintesis optimum dianalisis menggunakan spektroskopi fotoluminesens (PL) dan UV-Vis. Sampel disediakan melalui kaedah bantuan gelombang mikro. Kesan sifat optik pada spektrum PL dan UV-Vis diperhatikan dengan menukar isipadu Fe_3O_4 antara 0.2, 0.4, dan 0.6 ml. Untuk sintesis PbS/Fe_3O_4 CSQDs, suhu yang digunakan ialah 55 °C, dan campuran telah disinari dengan gelombang mikro selama 2 minit. Keputusan telah menunjukkan dengan jelas bahawa PbS/Fe_3O_4 membenarkan peralihan ciri optik kepada tenaga pelepasan yang lebih tinggi apabila isipadu Fe_3O_4 meningkat. Anjakan biru dalam PL ini difahami sebagai penghijrahan ion dan pertukaran mekanisme yang berlaku semasa sintesis. Daripada analisis spektrum PL, jurang jalur tenaga PbS dan PbS/Fe_3O_4 (0.2, 0.4, kepada 0.6 ml) masing-masing bertukar kepada 0.77, 2.67, 2.68, dan 2.74 eV. Walau bagaimanapun, analisis jurang jalur tenaga PbS dan PbS/Fe_3O_4 melalui UV-Vis masing-masing telah ditukar kepada 4.85, 3.61, 3.75, dan 4.0 eV untuk PbS dan PbS/Fe3O4 (0.2, 0.4, dan 0.6

ml),. Perbezaan tenaga antara PL dan UV-Vis ini disebabkan oleh anjakan Stoke berlaku dalam CSQD PbS/Fe_3O_4.

ACKNOWLEDGEMENT

First and foremost, praises and thanks to the God, the Almighty, for His showers of blessings throughout my research work to complete the research successfully.

I would like to express my deep and sincere gratitude to my research supervisor Dr Mazliana Ahmad Kamarudin for giving me the opportunity to do research and providing invaluable guidance throughout this research. Her dynamism, vision, sincerity and motivation have deeply inspired me. She has taught me the methodology to carry out the research and to present the research works as clearly as possible. It was a great privilege and honor to work and study under her guidance. I am extremely grateful for what she has offered me. I am extending my heartfelt to thanks her for her time and patience during the discussion I had with her on research work and thesis preparation.

I am extremely grateful to my parents Ambok Dalek and Mariani for their love, prayers, caring and sacrifices for educating and preparing me for my future. I am very much thankful to my parents and family for their valuable prayers and continuing support to complete this research work.

I would like to say thanks to my seniors Safwan and Kak Diyana for helping me in conducting the experiment in the lab. Also, thanks to them for sharing their knowledge about quantum dots and demonstrating the experiment to me.

I am extending my thanks to my research colleagues Fadhil and Adlin for helping me a lot throughout this semester. We both spend time together in the lab and cooperate with each other to synthesis the quantum dots. I am extremely grateful for their cooperative behavior.

Finally, my thanks go to all the people who have supported me to complete the research work directly or indirectly.

TABLE OF CONTENT

LIST OF FIGURES

LIST OF TABLES

LIST OF ABBREVIATION

QDs	Quantum Dots
CSQDs	Core Shell Quantum Dots
PbS	Lead Sulphide
Fe_3O_4	Iron Oxide
QYs	Quantum yields
UV	Ultraviolet
IR	Infrared
NIR	Near Infrared
CIS	Chlorosulfur
ZnS	Zinc Sulfide
$CdTe_xSe_{1-x}/CdS$	Cadmium Telluride selenide
CdS	Cadmium Sulfide
UV-Vis	Ultraviolet-Visible
CdSe	Cadmium Selenide
ZnSe	Zinc Selenide
In_2O_2	Indium Oxide
In_2S_3	Indium Sulfide
$Cd_xZn_{1-x}S$	Cadmium Zinc Sulfide
CdSe	Cadmium Selenide
ZnS	Zinc Sulfide
CdS	Cadmium Sulfide
SILAR	Successive Ionic Layer Adsorption and Reaction
PLE	Photoluminiscence Excitation
ML	Monolayer
TEM	Transmission Electron Microscopy
QLEDs	Quantum Dots Light Emitting Diodes
DI water	Deionized water

Ag	Silver
PdS	Palladium Sulfide
FHWM	Full Half Width Maximum
PXRD	Powder X-ray Diffraction
$PbCl_2$	Lead Chloride
OLA	Oleylamine
NPs	Nanoparticles
XRD	X-ray Diffraction
$Pb(C_2H_3O_2)_2$	Lead Acetate
TGL	1-Thioglycerol
DTG	2,3-Dimercaptopropanol
$FeCl_3$	Iron (III) Chloride Hexahydrate
KI	Potassium Iodide
N_2	Nitrogen Gas
NaOH	Sodium Hydroxide
DPSS	Diode-pumped solid-state
XPS	X-Ray Photoelectron Spectroscopy
XAS	X-Ray Absorption Spectroscop
TXRF	Total Reflection X-Ray Fluorescence

CHAPTER 1

INTRODUCTION

The first chapter will discuss the definition of quantum dots, its properties such as average size, and also its general applications. Furthermore, the first chapter will also introduce the general knowledge of core shell quantum dots including 4 types of quantum dots and its explanation. After that, the properties of PbS and Fe_3O_4 will also be discussed such as size and crystal structure. Lastly, the discussion will continue with problem statements and objectives of the research.

1.1 Quantum Dots

In recent studies, colloidal quantum dots (QDs) are said to have special optical properties regarding quantum confinement effects that have attracted a great inquisitiveness among the researchers in which the colloidal QDs' energy can be tuned by adjusting their particle size (Manzoor et al., 2009; Moreels et al., 2009). According to Alizadeh-Ghodsi et al. (2019) QDs can be defined generally as tiny particles having diameters ranging from 2 to 10 nm and offer a unique optical property. The unique optical property of QDs is because the colour of the QDs changes when the size of the QDs is changed (Manzoor et al., 2009) i.e. size-tunable light emission (Jin et al., 2011). In biological and chemical experiments, they have significant advantages over conventional fluorescent organic dyes in terms of photostability, signal brightness, and tunable emission spectra (Jin et al., 2011).

In general, electrons in the semiconductor can move from valence band to conduction band when they are excited by photons (J.M.K.C. Donev et al., 2018)[1]. While electrons are

excited to the conduction band, they will leave holes behind at the valence band which create an exciton (electron-holes pair). The distance between the electron and the holes is known as exciton Bohr radius. As the electron is excited to the conduction band, it will be in an unstable state. Thus, it will recombine back with the holes in the valence band. This recombination will cause the electron to emit some wavelength. The wavelength emitted is varying based on the energy band gap of the QDs. These properties of QDs are due to the tunable band gap which can be regarded as a semiconductor. Basically, a semiconductor having a band gap that can be tuned according to one's need by changing the physical properties of the semiconductor material/particles such as changing the size of the semiconductor material. (Smith & Nie, 2010)

1.2 Core/Shell QDs (CSQDs)

Core/shell QDs formed when the core of the QDs is coated with a shell from different semiconductor material. The presence of the shell can act as a physical barrier between the core and the vicinity (Reiss et al., 2009). Furthermore, the shell also passivates effectively the surface trap states, resulting in a significantly enhanced fluorescent quantum yield (Reiss et al., 2009). Besides that, the presence of the shell can also prevent photo-degradation processes from occurring in the inner QDs (Smyder & Krauss, 2011). The energy band gap of the shell can be wider or narrower than the core which form many types of the CSQDs as discussed in the following.

Initially, there are 4 types of CSQDs which are type-I, reverse type-I, type-II, and reverse type-II (Reiss et al., 2009) as shown in Figure 1.2.a, Figure 1.2.b, Figure 1.2.c, and Figure 1.2.d.

For type-I, both electrons and holes are confined in the core because the bandgap of the shell material is higher than that of the core. By passivating the surface of QDs, the primary objective of producing type-I structures is to enhance fluorescence Qys and photostability (Da et al., 2012).

In contrast to type-I, the bandgap of the core is higher than the band gap of the shell for reverse type-I. Hence, the electrons and the holes are at least partially delocalized in the shell and the emission results from the radiative recombination of exciton in the shell (X. Jin et al., 2017). A significant red-shift of the band gap will be observed and overcoating a shell material with a smaller band gap over a core material with a larger band gap might create nanocrystals with tunable emission colours (Zhong et al., 2005). According to (Zhong et al., 2005), the band gap energy reverse type-I is determined by the radius of the core, the thickness of the shell, the effective masses of the charge carriers in each material and the materials' conduction band offsets.

On the other hand, type-II core/shell structures promote carrier separation by engineering band offsets to necessitate charge transfer at the core/shell interface (Smyder & Krauss, 2011). The valence-band edge or the conduction-band edge of the shell material is lying in the band gap of the core for type-II structures, resulting in staggered band offsets (Da et al., 2012).

Apart from that, reverse type-II having the valence band edge of the shell lies within the band gap of the core or conduction band edge of the core lies within the band gap of the shell (Chuang et al., 2010).

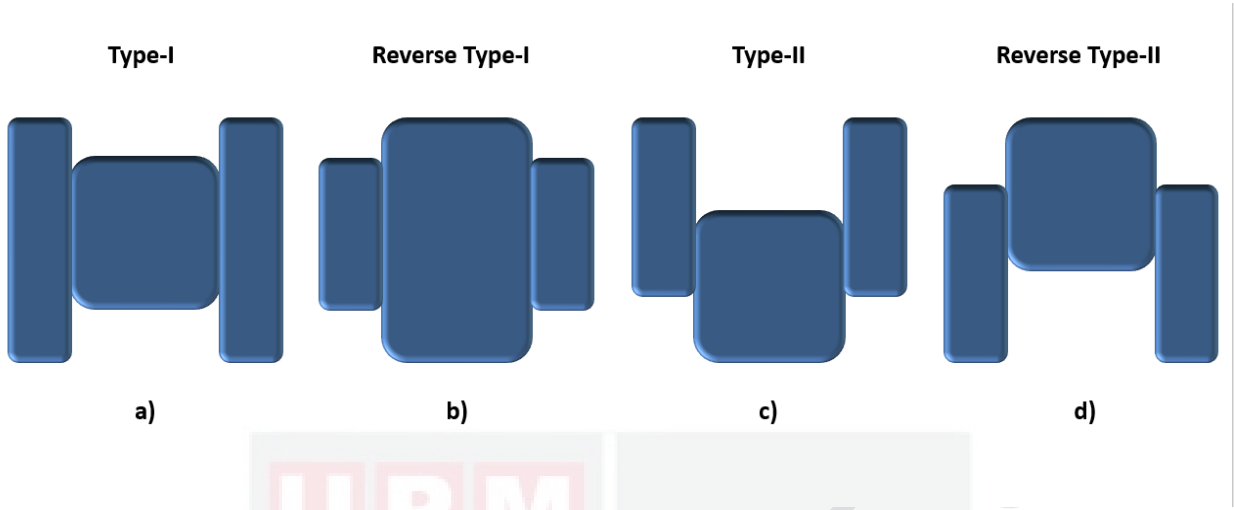

Figure 1.2 The energy band gap of different type of QDs

1.3 Properties of Lead Sulphide

Lead sulphide (PbS) belongs to IV-VI group chalcogenides semiconductor (Ezekoye et al., 2015). According to Román-Zamorano et al. (2009), lead sulphide (PbS) nanoparticles have an average size of roughly 10 nm. The compound semiconductor PbS has a bulk energy bandgap of 0.41 eV (Mozafari & Moztarzadeh, 2010) with a large exciton Bohr diameter of 18 nm (Moreels et al., 2009). Moreover, PbS has a crystal structure of cubic rock salt structure as shown in Figure 1.3 with the lattice constant a = 0.59362 nm at normal atmospheric pressure and room temperature (Sadovnikov et al., 2016).

PbS QDs are toxic in nature as they contain toxic components which are Pb^{2+} which induce potential biological toxicity (Mozafari & Moztarzadeh, 2010). Moreover, PbS QDS have high photostability, wide UV excitation, bright fluorescence, and narrow emission which have

higher advantages than fluorescent dyes utilized in biological imaging (Mozafari & Moztarzadeh, 2010). Apart from that, according to experimental literature data, the time-resolved luminescence spectroscopy shows that the exciton lifetime ranging between 1 and 3 μs (Moreels et al., 2009).

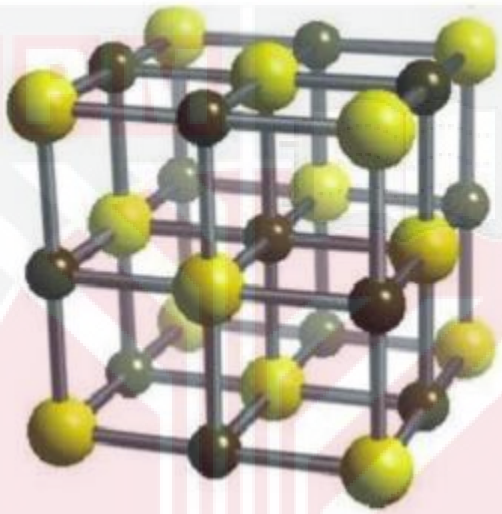

Figure 1.3 The crystal structure and symmetry of PbS (Yin, 2018)

1.4 Properties of Iron Oxide

Based on the result of previous research, the size of uniform iron oxide nanoparticles is ranging from 10-24 nm (Patsula et al., 2016). The structure of iron oxide (Fe_3O_4) is an inverse spinel where the smaller Fe cations occupy octahedrally and tetrahedrally coordinated interstices in between, which are all based on a closed packed O_2-anion lattice (refer Figure 1.4) (Parkinson, 2016). The lattice constant of Fe_3O_4 is a = 0.8396 nm and the colour of Fe_3O_4 is black (Parkinson, 2016). According to (Tian et al., 2011), the bulk energy of Fe_3O_4 is 0.1 eV.

Essentially, Fe_3O_4 exhibits absorption in the visible and near-IR regions due to thermally induced electronic transitions assigned to intervalence charge transference (Martinez et al., 2015). Apart from that, Fe_3O_4 also exhibits special properties such as easy separation methodology, surface-to-volume ratio, superparamagnetic, and larger surface area (Zia et al., 2016).

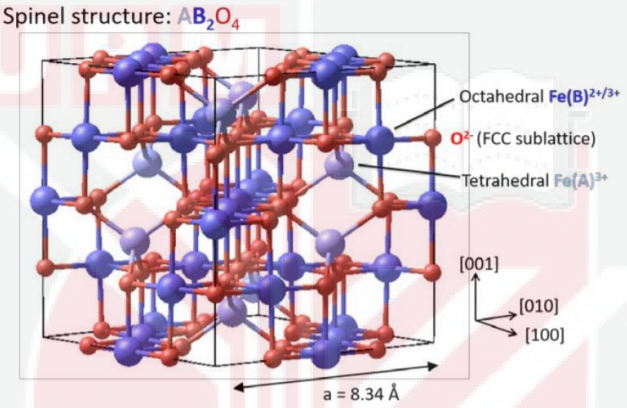

Figure 1.4 The crystal structure of Fe_3O_4 (Parkinson, 2016)

1.5 Problem Statement

In recent years, scientists are fascinated by QDs because of their simultaneous targeting and imaging potential in biological applications, pharmacological, and drug delivery (Bajwa et al., 2016). Previously, for biological applications, fluorescence imaging of biological systems can be observed by using common probes such as organic dyes (Gil et al., 2021). Unfortunately, many organic dyes are limited by the fact that their excitation and emission occur in the ultraviolet (UV) and visible range, which is outside the biological transparency windows which is near-infrared I (NIR-I) and near infrared II (NIR-II) (Gil et al., 2021). The wavelength region for NIR-I is 650 to 950 nm and NIR-II is 1000 to 1400 nm (Gil et al., 2021). This NIR biological windows is the ideal electromagnetic spectrum region for fluorescence imaging because the scattering, absorption, and auto-fluorescence from tissues is greatly reduced in this region. Hence, the image quality and tissue penetration will be improved.

However, the excitation and emission that lies within UV-visible range will create an autofluorescence produced by tissues in the body which consequently produce images with low contrast and quality (Gil et al., 2021). Nowadays, QDs are particularly favorable than organic dyes for fluorescence imaging applications due to their unique properties such as size-tunable absorbance and emission, large Stokes shift, and high brightness (Gil et al., 2021).

In 2004, an experiment was conducted by Ballou et al. 2004 to study about vivo imaging using zinc sulfide-cadmium selenide CSQDs coated with an amphiphilic poly(acrylic acid) polymer (Ballou et al., 2004). The maximum wavelength of the CSQDs is 606, 630, 645, and 655 nm (Ballou et al., 2004). Furthermore, it is also being observed that the CSQDs have no

significant effects on tissue deposition or circulating lifetimes (Ballou et al., 2004). The experiment was conducted successfully as the CSQDs produced have high absorbency and high quantum yield as the CSQDs was readily visible to naked eyes (Ballou et al., 2004). However, the exciting or emitted light of QDs that emit fluorescence near visible light may be absorbed by water, fat, oxygenated hemoglobin, proteins, skin, and cell structures (Gil et al., 2021). Furthermore, CSQDs with fluorescent range near visible light will not be suitable for tissue with thickness more than 1 mm as it will not produce a good visualization (Ballou et al., 2004). The reason behind this is that the photons in the visible wavelength do not penetrate deeply within organic tissues (Gravier et al., 2012).

Another CSQDs used for bioimaging is CIS/ZnS CSQDs (Li et al., 2009). Generally, CIS/ZnS CSQDs is a type-I QDs where the ZnS shell has higher band gap energy than the CIS core which are 3.6 eV and 1.5 eV respectively (Li et al., 2009). Furthermore, CIS/ZnS CSQDs produce fluorescence of quantum yield of 60% and exhibit photoluminescence in the range of 550 to 815 nm which is favorable for vivo biological imaging as this application needs the probes to absorb and emit light in a spectral window of 650-900 nm to reduce light absorption and scattering by water and (oxy-)hemoglobin (Li et al., 2009). However, the CIS/ZnS CSQDs does not have superparamagnetic properties to improve its kinetics in vivo imaging (Stephen et al., 2011).

Apart from that, a red to near-infrared emitting CSQDs also has been prepared for biological imaging and detection (Jiang et al., 2006). This quantum dots is so called $CdTe_xSe_{1-x}/CdS$. This CSQDs have tunable wavelength from 600 to 850 nm. It is found that the quantum yield of $CdTe_xSe_{1-x}/CdS$ is roughly 35 to 40% which is bright enough to be imaged at individual

nanoparticle levels (Jiang et al., 2006). Although this CSQDs has emission lies in NIR biological windows, high quantum yields (>30%), narrow spectral linewidths (<50 nm), and high stability against photobleaching, the kinetics of this CSQDs can still be improved by developing a superparamagnetic property in it (Stephen et al., 2011).

However, there is less emission near infrared range for reverse type-I CSQDs for bioimaging applications.

1.6 Objective of the research

The objectives of this research are:

I. To synthesis colloidal PbS QDs and PbS/ Fe_3O_4 CSQDs with different volume of iron oxide via the microwave-assisted method

II. To examine the optical properties of PbS QDs and PbS/Fe_3O_4 CSQDs with different volume of Fe_3O_4 by using photoluminescence (PL) spectroscopy and UV-Vis's spectroscopy

CHAPTER 2

LITERATURE REVIEW

2.1 Nanoparticle Reverse Type-1

Generally, CSQDs of reverse type-I can be produced by using different compounds with the shell having lower energy band gap and coating the core with higher energy band gap. A few compounds have been used to produce CSQDs of reverse type-I by previous researchers such as CdS/CdSe (Battaglia et al., 2003), ZnSe/CdSe (Zhong et al., 2005), In_2O_3/In_2S_3 (Sun et al., 2008), $Cd_xZn_{1-x}S$/CdSe (Jin et al., 2017), and ZnS/CdS (Shariati et al., 2018).

The experiment of synthesis CdS/CdSe CSQDs is conducted by coating different monolayers (ML) of CdSe shell with different size of CdS core by using Successive Ionic Layer Adsorption and Reaction (SILAR) technique. The newly discovered SILAR technique is developed by the alternating introduction of precursors for the anionic and cationic components of the shell compound semiconductor (Battaglia et al., 2003). The experiment is conducted by growing the CdSe shell from 3-layer, 5-layers, to 7-layers on CdS core with diameters between 2.5 and 5.0 nm. The average energy band gap of CdS is calculated to be 2.80 eV (Mansur et al., 2011) whereas the energy band gap of CdSe is calculated to be 2.55 eV (Kapatkar et al., 2018). It was reported that the CdS/CdSe CSQDs have a wide range of adjustable emission colours that encompass the majority of the visible optical window (Battaglia et al., 2003). The absorption peak was observed ranging from 380 to 440 nm. From photoluminescence excitation (PLE) spectra, it shows that the absorption feature is indeed caused by the CdSe shells. Furthermore, it was observed that the highest PL quantum yield (QY) of the CdSe quantum shells' band-edge

emission was around 20%. Nevertheless, the QY can be enhanced through inorganic passivation by epitaxial development of a high bandgap energy semiconductor on the quantum shells' surface in a one-pot approach. Consequently, the PL QY was significantly increased and the PL peak was shifted to higher wavelength.

Another experiment of synthesis reverse type-I CSQDs is synthesis of ZnSe/CdSe by using modified literature method to produce ZnSe Core and mixed with Cd and Se precursor (Zhong et al., 2005). The addition of Cd/Se precursor was added slowly to ensure a heterogeneous grow occurred onto the existing ZnSe nuclei. The bulk energy band gap of ZnSe is found to be at 2.58 eV whereas the bulk energy band gap of CdSe is 1.74 eV (Zhong et al., 2005). The experiment was conducted by varying the thickness of the CdSe shell from 0.1, 0.2, 0.5, 1, 2, 3, 4 and 6 ML onto the ZnSe core with an average size of 2.8 nm. The shell thickness was controlled by the addition rate of the precursors. It was observed that both the band-edge PL emission peaks in the PL spectra and the absorption onsets in the absorption spectra change consistently to the red as the CdSe shell thickness around the ZnSe cores increases. The PL peak was changed from 418 to 674 nm as the shell thickness increases from 0.1 to 6 ML. By the addition of Se and Cd precursors to a diluted ZnSe nanocrystals reaction solution, it will result in extremely luminous QY from 40 to 85 percent. The overcoating of CdSe shell onto the ZnSe core will affect the emission colors to sequentially adjusted from violet to red. Apart from that, ZnSe can crystalize in zinc-blende structure or wurtzite structure (Wang et al., 2015) whereas the CdSe shell is preferentially form the wurtzite (hexagonal) structure (Zhong et al., 2005).

Next, the other experiment of synthesizing reverse type-I is about In_2O_3/In_2S_3 CSQDs by using a one-pot synthesizing method (Sun et al., 2008). From the Transmission Electron

Microscopy (TEM) image, it shows that the In_2O_3 core resulted from this experiment possesses an average diameter of 10 nm with the entire core-shell diameter is 16 nm (Sun et al., 2008). The energy band gap of In_2O_3 is 3.6 eV while the bulk energy band gap of In_2O_3 is ranging from 2.00 to 2.30 eV (Sun et al., 2008). From X-ray spectrum (EDS) analysis, it was observed that the molar ratio between In_2S_3 and In_2O_3 was around 2.2 : 1 to 3.6 : 1. Under ambient condition, the crystal structure of In_2O_3 is cubic bixbyite-type (Bierwagen, 2015; Liu et al., 2013) while the crystal structure of In_2O_3 is defect spinel-type structure (309-704 K), cubic crystal structure (749-1044 K), and layered structure (1099-1322 K) (Pistor et al., 2016). Additionally, the photoluminescence for both In_2O_3 QDs and In_2O_3/In_2S_3 CSQDs indicates the same emission peaks centered at 422, 440, 461, 484and 533 nm when excited with excitation wavelength of 233 nm. Thus, when excited in the far UV region, the PL emissions was in the near UV and visible area. The further analysis of PL spectra of this CSQDs will be discussed in the next part which under photoluminescence part. This In_2O_3/In_2S_3 CSQDs was reported could produce high anodic photocurrent when this CSQDs applied as electrodes to be used in solar cells and optoelectronic application.

Next, an experiment is conducted by Jin et al. to synthesize $Cd_xZn_{1-x}S/CdSe$ which belong to reverse type-I. The CSQDs was prepared to produce an efficient light emitting diode so called quantum dots light emitting diode (QLEDs). Initially, the synthesizing is conducted by utilizing the method used by Lee et al. but with some modification (X. Jin et al., 2017). The band gap of $Cd_xZn_{1-x}S/CdSe$ is about 3.0 eV and the band gap of CdSe is 1.82 eV (X. Jin et al., 2017). The experiment is conducted by varying the thickness of CdSe shell from 1, 1.5, 2, 2.5, 3 and 4 ML onto the core. From the conducted experiment, the average diameter of the $Cd_{0.1}Zn_{0.9}S$ core is

estimated to be around 4.5 nm and raised to 6.5 nm when a 2 ML CdSe shell is overgrown onto $Cd_{0.1}Zn_{0.9}S$ core based on statistical data from ten TEM pictures. This shows that the thickness of 1 ML of CdSe is 0.1 nm. As the thickness of the CdSe shell is increasing, a notable red-shift of the absorption and PL spectra are observed. Depending on the thickness of the CdSe shell, the resultant QDs emit bright full colour emissions ranging from blue to red. Apart from that, it was reported that this CSQDs is experiencing a small stoke shift around 15 nm between the emission peaks and the corresponding first excitonic absorption which indicates that the reverse type-I $Cd_{0.1}Zn_{0.9}S$/CdSe system favours band-edge luminescence over deep trap emission at long wavelengths, which is necessary for high emission efficiency. Furthermore, $Cd_xZn_{1-x}S$/CdSe possesses two crystal structures which are wurtzite and zinc blende structure (Xu et al., 2014) while CdSe forms in wurtzite (hexagonal) structure (Zhong et al., 2005). Eventually, the prepared $Cd_xZn_{1-x}S$/CdSe CSQDs is having a wide tunable emission ranging from 450 to 670 nm and a quantum yield of 61% at 638 nm which is well-established to developed highly efficient QLEDs.

Lastly, another reverse type-I CSQDs was been synthesized which is ZnS/CdS CSQDs (Shariati et al., 2018). The CSQDs was prepared by using precipitation method where the solution containing Zn precursor is mixed with solution containing S and Cd precursor accordingly until the precipitates forming at the end of the mixture is collected, washed, dried in oven and eventually resuspended in DI water (Shariati et al., 2018). The bulk energy band gap of ZnS is found to be 3.68 eV (Uzar & Arikan, 2011) whereas the bulk energy band gap for CdS is 2.42 eV (Qutub & Sabir, 2012). It was analyzed that the size of this CSQDs is 8.0 nm. Furthermore, the CSQDs absorption spectra shows double bands at 310 and 425 nm. Moreover,

under PL spectra, the CSQDs shows a single fluorescence peak at 500 nm by using excitation value of 300 nm (Shariati et al., 2018). The CSQDs is later loaded by Ag and PdS co-catalyst to enhance the performance and photostability of CSQDs to be used for photocatalytic antibacterial applications.

All in all, the purpose of synthesizing many compounds in the same reverse type-I is to change PL properties and QY for the sake of its application.

2.2 Quantum Yield

According to Sadjadi (2021) QY refers to the effectiveness of turning absorbed light into emitted light, which might be in the form of fluorescence. In this section, all the reverse type-I CSQDs stated before will be discussed about their QY.

The highest QY of CdS/CdSe CSQDs is found to be around 20% which corresponds to the size ranging from 6.0 to 8.5 nm (Battaglia et al., 2003). The lower QY is due to deep-trap emission resulted by the energy level that act as a deep-trap state of a single monolayer with narrow bandgap (Battaglia et al., 2003). In order to improve the quantum yield, one can use inorganic passivation additional epitaxial growth of a high bandgap semiconductor on the surface of the quantum shells via one-pot approach (Battaglia et al., 2003).

Another experiment of reverse type-I is about ZnSe/CdSe Core/Shell nanocrystal. The QY for the original core particle ZnSe is about 40% (Zhong et al., 2005). As the ZnSe core is coated with CdSe shell with increasing thickness, the QY of the core/shell nanocrystal reaches the highest value of 85% until the shell thickness is 3 ML (Zhong et al., 2005). If the shell thickness is

increasing more than 3 ML, the QY will decrease gradually until 25% at shell thickness of 6 ML (Zhong et al., 2005). This case may be due to a weaker quantum confinement effect caused by their larger particle sizes (Zhong et al., 2005). At 6 ML, the particle radius is 3.5 nm which is close to the value of corresponding exciton Bohr radius of ZnSe (4.5nm) and CdSe (5.4nm) (Zhong et al., 2005).

Next, for another reverse type-I CSQD which is In_2O_3/In_2S_3 the author does not state the QY of the CSQDs. Instead, the author reported the PL of the In_2O_3/In_2S_3 CSQDs which will be discussed in the next section

Next, according to Jin et al. (2017) he reported that the QY of the $Cd_xZn_{1-x}S$ core is 11%. After the core is coated with different thickness of CdSe, the increase of QY is observed where the highest QY of $Cd_xZn_{1-x}S$/CdSe is 61% at thickness of 3 ML of CdSe shell (Jin et al., 2017). However, as the CdSe grows, the QY decreases as observed for CdSe shell with thickness of 4 ML having QY of 28% (Jin et al., 2017). Jin et al. predicted that the declining of QY is due to the thickness of the shell may exceed the exciton Bohr radius of CdSe (5.4 nm) and result in weaker quantum confinement effect (Jin et al., 2017).

Lastly, the QY of ZnS/CdS CSQDs also not been being stated by the author. Its PL spectra however, will be discussed in the next section.

2.3 Photoluminescence@Optical properties

For CdS/CdSe CSQDs, the PL spectra changes as different shell thickness of CdSe coat the CdS core. On the other hand, PL and absorption spectra show astonishingly similarity if the

same thickness of CdSe shell is overgrown onto different size of CdS core. Battaglia et al. (2003) reported that the position of the PL peak and the colour of the emission were both substantially dependent on the thickness of the quantum shells for shells with a thickness equal or higher than two monolayers (Figure2.3a).

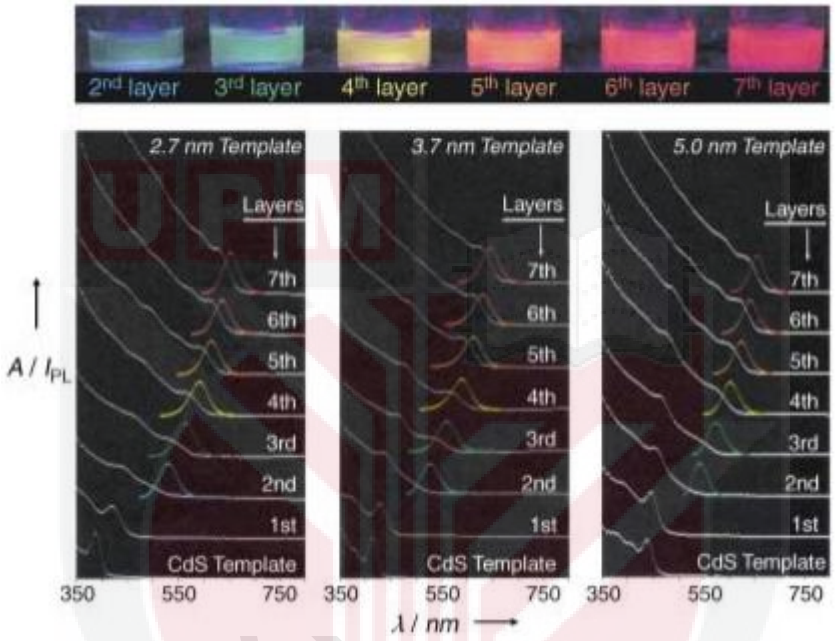

Figure 2.3a Top: emission colors of CdS/ CdSe quantum shells with different shell thicknesses; Bottom: Absorption and PL spectra of the CdSe quantum shells grown on three different-sized CdS templates, 2.7 nm (left), 3.7 nm (middle), and 5.0 nm (right). The number of CdSe monolayers is marked on the right for each sample (Battaglia et al., 2003).

It is observed a significant redshift occurred in PL and absorption spectra where the range is in UV-Visible light (Battaglia et al., 2003).

The other experiment about reverse type-I is the experiment about ZnSe/CdSe Core/Shell nanocrystals. The energy band gap of ZnSe and CdSe is 2.58 eV and 1.71 eV

respectively (Zhong et al., 2005). This indicates that the shell has a lower energy band gap than ZnSe which can be regarded as reverse type-I nanocrystal. It was reported that the emission colours of the CSQDs may be adjusted sequentially from violet to red by overcoating the CdSe shell onto the ZnSe cores. As the CdSe shell thickness increases around the ZnSe core, the PL peak emission demonstrates a redshifted (lower band gap energy) (Zhong et al., 2005). The CdSe thickness is set to increase from 0.1, 0.2, 0.5, 1, 2, 4, and 6 ML resulting in an increase of PL peak from 418, 473, 515, 566, 614, 654, and 674 nm respectively. The whole visible spectrum from the violet to the red is covered by the PL emission from these core/shell nanocrystals as being shown by Figure 2.3b (Zhong et al., 2005).

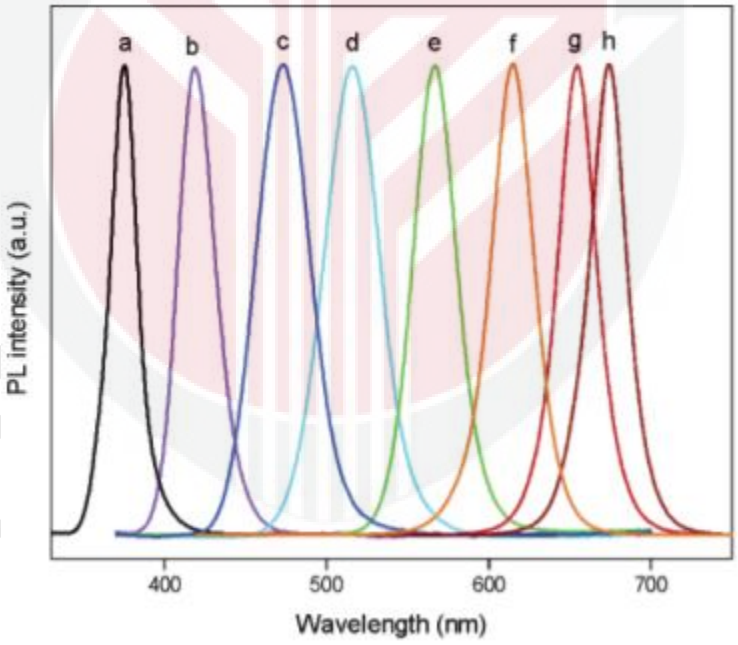

Figure 2.3b Normalized PL (left, λ_{ex} for ZnSe =320 nm, for ZnSe/CdSe = 360 nm) and corresponding absorption (right) spectra of plain ZnSe core nanocrystals (a) and ZnSe/CdSe core/shell nanocrystals with different numbers of monolayers of CdSe shell: b, 0.1; c, 0.2; d, 0.5; e, 1; f, 2; g, 4; h, 6 (Zhong et al., 2005).

Furthermore, another experiment of reverse type-I CSQDs has been done which involves indium oxide (In_2O_3) as the core and indium sulfide (In_2S_3) as the shell (Sun et al., 2008). The synthesis of In_2O_3/In_2S_3 CSQDs is using one-pot method and produces CSQDs with shell thickness of about 4 nm (Sun et al., 2008). Both In_2O_3 QDs and In_2O_3/In_2S_3 CSQDs shared the same PL spectra where multiple emission peaks centered at 422, 440, 461, 484, and 533 nm with an excitation wavelength of 233 nm but with different intensities where In_2O_3/In_2S_3 CSQDs is having higher intensity compared to In_2O_3. In other word, when the CQDs is stimulated in the far ultraviolet (UV), the PL emissions are in the near UV and visible area as been shown in Figure 2.3c.

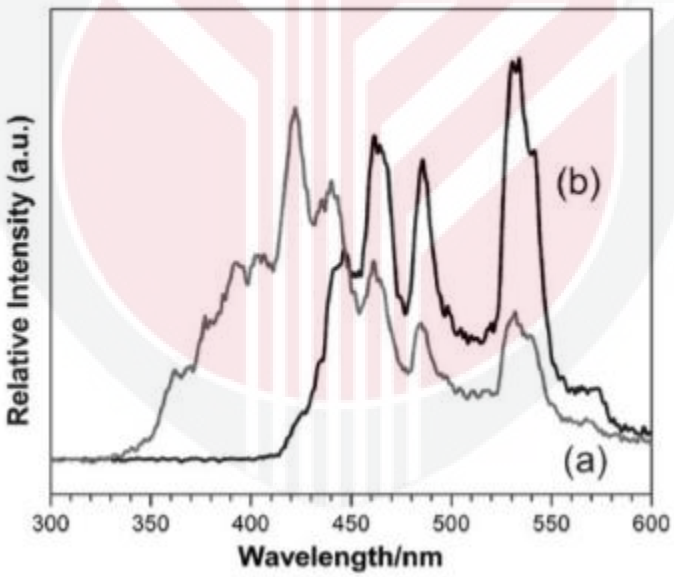

Figure 2.3C Photoluminescence spectra of (a) In_2O_3 nanocrystals; and (b) In_2O_3/In_2S_3 core–shell nanoparticles suspended in hexane (Sun et al., 2008).

It can be related that the In_2S_3 shell does not modify the places of In_2O_3 emission, rather it does vary the relative intensities of the emissions. Sun et al. explained that the emission at 422 nm and 440 nm is attributed to near band-edge emission, whereas the other peaks are

attributed to oxygen deficit. The result of this experiment has shown that the photoluminescence spectra of this CSQDs reverse type-I is at emission of 442 and 440 nm which corresponds to visible wavelengths (Sun et al., 2008).

From the experiment of $Cd_xZn_{1-x}S$/CdSe core/shell, significant red changes in the absorbance and PL spectra have been observed, proving the development of CdSe shell. Depending on the thickness of the CdSe shell, the resulting QDs emit bright full colour emissions ranging from blue to red when the thickness of the CdSe shell increases. The data collected from the absorption spectra shows that as the thickness increases from 1 ML to 4 ML the PL peak wavelength also increases from 556 nm to 635 nm as shown in Figure 2.3d.

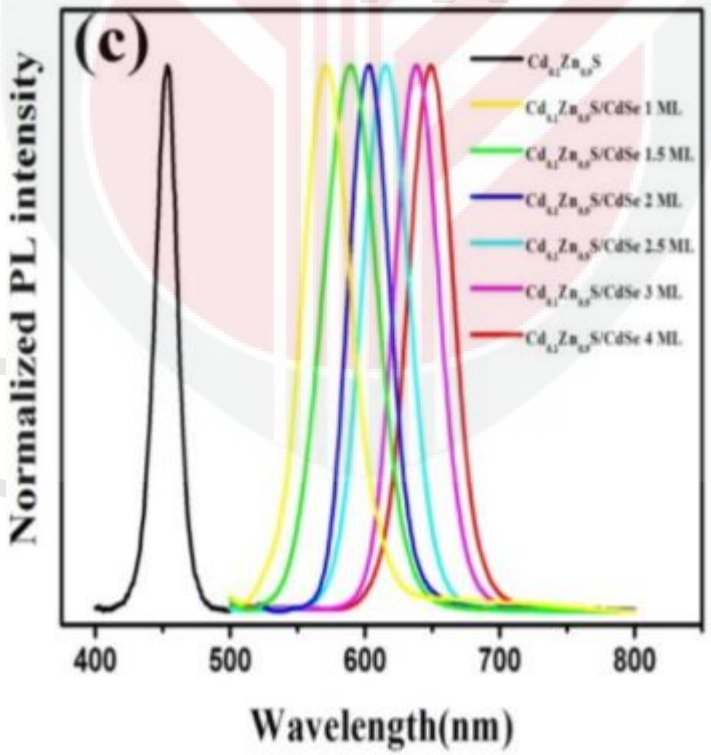

Figure 2.3d PL spectra of the $Cd_xZn_{1-x}S$/CdSe core/shell CSQDs (Jin et al., 2017).

This indicates that as the shell thickness is increasing, then the energy band gap of the shell also increases and hence prove the reverse type-I. On the other hand, the analysis of PL shows that the PL curves become symmetric as the shell thickness increases, and the full width at half maximum (FWHM) decreases from 45 to 30 nm, demonstrating that size focusing occurs throughout the shelling process. However, as the thickness of the CdSe shell increases more than 3 ML (>3ML), the FWHM increases and the QY starts to decline due to weaker quantum confinement effect as the thickness of the shell may be more than the CdSe exciton Bohr radius (Jin et al., 2017).

However less works have been done on core shell QDs reverse type-I at near infrared emission

2.4 Synthesis of PbS QDs

In recent years, PbS quantum dots are interestingly being investigated by many researchers due to its simplicity of synthesis (Hines & Scholes, 2003, as cited in Zhang et al., 2014), strong quantum confinement (Wise, 2000, as cited in Zhang et al., 2014), and favourable quantum confinement effects including multiple exciton formation (Nozik et al., 2010, as cited in Zhang et al., 2014). There are a few different methods to synthesize Colloidal PbS quantum dots.

In 2006, an experiment conducted by Cademartiri et al., to produce high-quality PbS nanocrystals in multigram-scale quantities via hot-injection synthesis. This synthesis is able to produce good quality and unprecedented monodispersity of PbS as shown by a FWHM of the PL

peak as low as 52 meV. Furthermore, the QY produce by the PbS Qds is 40% and the Stokes shift as low as 10 meV (Cademartiri et al., 2006). However, because of the comparatively low nucleation threshold with S:OLA, this reaction method works well for larger QD sizes but fails to form QDs with diameters less than 3 nm (Zhang et al., 2014).

Hence, an experiment conducted by Zhang to develop a simple non-hot-injection synthetic route that achieves *in situ* halide-passivated PbS and PbSe quantum dots (QDs) (Zhang et al., 2014). *In situ* halide-passivated PbS QDs with a narrow size distribution (smaller than 3 nm) are produced from this method. During the experiment, the parameter being observed is the effect of temperature on the QDs. It is found that the QDs grow as the temperature increases. Additionally, when compared to traditional synthesis, the PL QY of PbS QDs is 30% greater when using this method.

For colloidal PbS quantum dots, a low-cost, large-scale synthetic approach was established (Huang et al., 2017). The produced QDs have great air-stability of at least 60 days and high PL QY of >40%. Furthermore, with a high chemical yield of 80%, the synthesis was easily scaled up to produce 18 g PbS QDs from a single batch of reaction.

Another way of synthesizing colloidal PbS quantum dots is by synthesizing PbS QDs using $PbCl_2$ in oleylamine (OLA) (Cademartiri et al., 2006). A single phase of PbS is produced at the end of the experiment after being analyzed with Powder X-ray Diffraction (PXRD). Furthermore, TEM analysis also demonstrates that the PbS QDs produced are having high monodispersity and colloidal stability (Cademartiri et al., 2006).

2.5 Synthesis of Fe_3O_4 shell

In recent years, Fe_3O_4 has received enthusiastic attention from my researchers due to its magnetic properties. There are many methods of synthesizing Fe_3O_4.

One of the methods is called coprecipitation method. This method is a cost-effective method, most efficient and the simplest among other methods (Kalantari et al., 2014). Although all the pros stated, there are a few major drawbacks of this coprecipitation method which are coaggregation of nanoparticles, easy oxidation/dissolution of magnetic nanoparticles, and difficulty recycling such tiny nanoparticles (NPs) (Kalantari et al., 2014).

Another way of synthesizing Fe_3O_4 is by a method called hydrothermal method conducted by Lei et al. in 2017. The hydrothermal process is particularly appealing because of various advantages such as cost-effective and environmentally friendly, materials with superior crystallinity and particle size, and morphologies that can be controlled. The final product of this experiment is octahedral particles of Fe_3O_4. Moreover, the results from XRD pattern indicate that the product of Fe_3O_4 produced from hydrothermal method is having a high purity and crystallinity as there is no peak assigned to any impurities observed (Lei et al., 2017).

Apart from that method, there is also another way to produce Fe_3O_4 which is sol–gel route. This method can produce a large scale of Fe_3O_4 nanoparticles and provide a simple way to do it (Cui et al., 2013). The benefit of this method is it will produce a solution of iron oxide with homogeneous nucleation (Cui et al., 2013).

CHAPTER 3

METHODOLOGY

This chapter will explain about the materials involved in synthesization of PbS, Fe_3O_4 and PbS/Fe_3O_4 CSQDs. Apart from that, this chapter will also explain the method on how PbS, Fe_3O_4, and PbS/Fe_3O_4 CSQDs are synthesized.

3.1 Materials

The list of materials utilized to synthesis PbS/Fe_3O_4 is shown in the Table 3.1

Material	Present State	Chemical Formula
Lead Acetate	Solid crystal	$Pb(C_2H_3O_2)_2\ 3H_2O$
Sodium Sulphide	Solid crystal	$Na_2S.\ 9H_2O$
Iron (III) chloride hexahydrate	Solid crystal	$FeCl_3.\ 6H_2O$
Potassium Iodide	Liquid	KI
Deionized water	Liquid	H_2O
Nitrogen gas	Gas	N_2
Sodium Hydroxide	Liquid	NaOH
1-Thioglycerol (TGL)	Liquid	$C_3H_8O_2S$
2,3-Dimercaptopropanol (DTG)	Liquid	$C_3H_8OS_2$

Table 3.1 List of materials used to prepare the sample

3.2 Preparation of PbS QDs

The PbS core is synthesized by the following method used by Zaini et al. which is a colloidal method (Zaini et al., 2020). Generally, PbS QDs are made of two precursors which are Pb^{2+} and S^{2-} where in the end we will mix both precursors to form PbS QDs. Initially, we are preparing 30 ml of Pb^{2+} and 2.7907 ml of S^{2-}. In order to prepare 30 ml Pb^{2+} precursor, firstly we dissolve 0.1889 g (0.0166 M) of $Pb(C_2H_3O_2)_2$ in deionized water at ambient temperature. The reaction was then degassed by removing oxygen from the flask via flowing nitrogen gas into it. After that, the Pb^{2+} precursor was mixed for 15 minutes.

In the two-neck flask containing Pb^{2+} precursor, 0.3885 ml TGL was introduced, followed by 0.1497 ml DTG. The colour of the solution then changed to a yellowish-green. To avoid agglomeration, the ligands TGL and DTG were added to the solution. Next, drop by drop, triethylamine was added to the solution until it reached pH 11 and the solution became colorless.

The two predecessors were then mixed together at 400 rpm with continuous stirring. The colour of the solution would then change from colourless to dark brown. PbS QDs were definitely formed as a result of this. The synthesis of PbS QDs with capping ligands is depicted schematically in Figure 3.2.

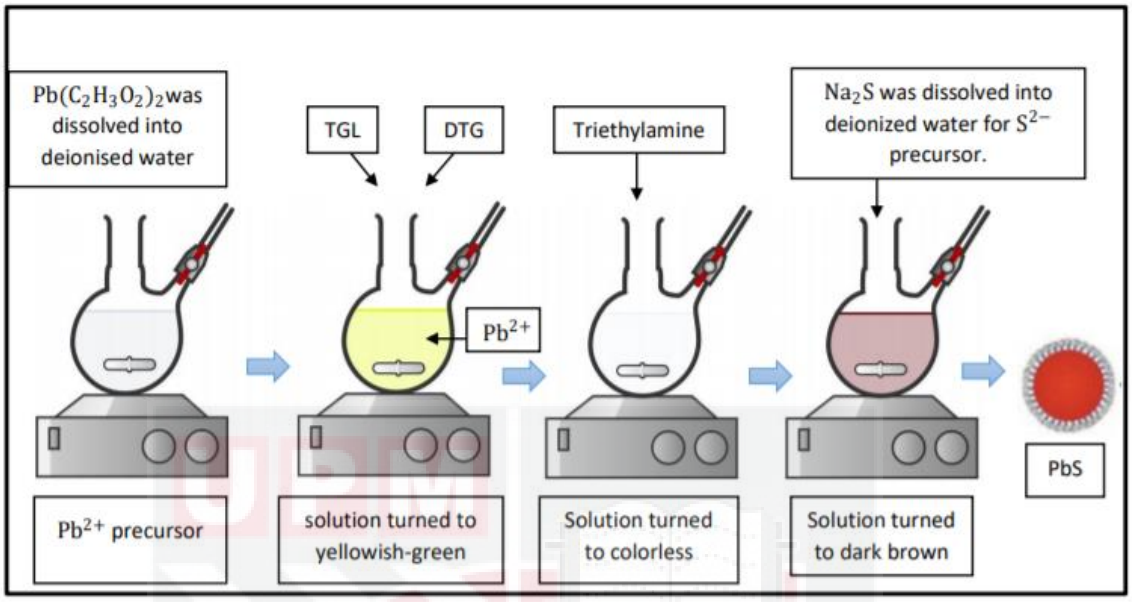

Figure 3.2 The schematic diagram of preparation of PbS QDs with the capping ligands (Noor Afifah, 2021)

3.3 Preparation of Fe_3O_4

The Fe_3O_4 shell is synthesized using the co-precipitation approach proposed by Khalil (Khalil, 2015). The first step is divided into two parts. First part is to dissolve 4.866 g (0.03 mol) of anhydrous $FeCl_3$ in 37.82 ml of distilled water. For the second part, 1.66 g (0.01 mol) of KI was dissolved in 12.63 ml of distilled water. After that, both dissolved $FeCl_3$ and dissolved KI are mixed together at ambient temperature, stirred. After that, at ambient temperature, both dissolved $FeCl_3$ and dissolved KI are mixed together, stirred, and allowed to attain equilibrium for one hour.

After one hour, precipitation of iodine will be formed. Hence, the precipitate iodine will be removed from the mixed solution by filtering it out using filter paper. Then, 76 ml of NaOH is dropped wisely to hydrolyze the filtrate with continuous stirring until it reaches pH 11 and precipitation of black magnetite is formed. After that, the setup is given an hour to settle. Consequently, two layers with a clear layer on the upper layer and black precipitate layer on the bottom appeared. The clear layer will be taken out by using a syringe and the black precipitate is then washed with distilled water and ethanol.

After washing, the black precipitate is dried under the sun to obtain Fe_3O_4 powder. The powder is then grounded and sieved. Afterwards, a sonicator is used to sonicate the mixture for 30 minutes. After being filtered, the colour of the precipitate changed to a light yellowish colour. The preparation of Fe_3O_4 shell is depicted schematically in Figure 3.3.

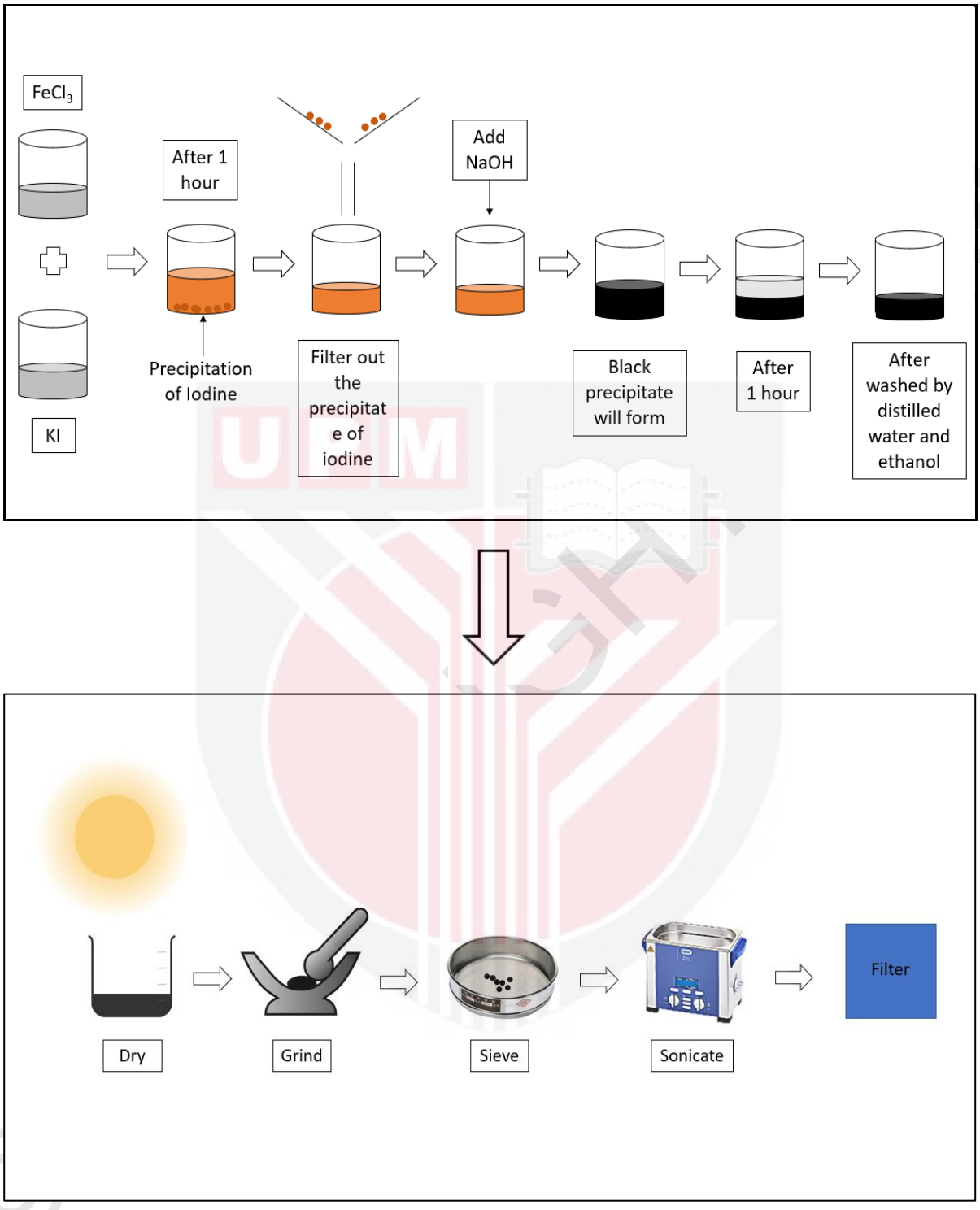

Figure 3.3 The schematic diagram for the preparation of Fe_3O_4 (Noor Afifah, 2021)

3.4 Preparation of PbS/Fe_3O_4 CSQDs

A microwave-assisted method is used to synthesize the PbS/Fe_3O_4 CSQDs. In this project, the microwave that we utilize is a Monowave 400/200 microwave reactor that can produce small-scale microwave synthesis applications. Then, take out 0.2, 0.4 and 0.6 ml of the filtered Fe_3O_4 and add it to a degassed glass tube with 5 ml of the prepared PbS QDs. At a constant temperature of 55 °C, the mixture is irradiated with microwave growth durations at 2 mins. The formed PbS/Fe_3O_4 CSQDs are then transferred to a degassed vial and stored at 4°C and away from light.

CHAPTER 4

RESULTS AND DISCUSSION

This chapter presents the optical characteristic of PbS quantum dots (QDs) and PbS/Fe_3O_4 core shell QDs (CSQDs). The result of Fe_3O_4 for Xray-diffraction (XRD), photoluminescence (PL) and UV-Vis spectroscopy will be discussed.

4.1 X-ray Diffraction (XRD) of Fe_3O_4

Figure 4.1 shows the XRD peak of Fe_3O_4. From the analysis, it was confirmed that our sample is a pure magnetite Fe_3O_4.

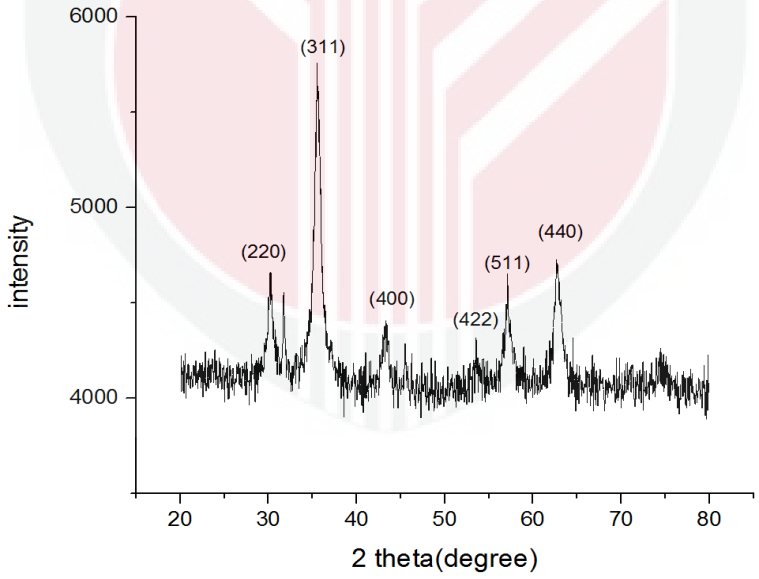

Figure 4.1 XRD analysis of Fe_3O_4

Our Fe_3O_4 shows a cubic crystal structure with lattice parameter a = 8.3750 Å which matched the standard data (JCPDS Card No 01-088-0315). Based on Figure 4.1, the Fe_3O_4 XRD pattern

consist of characteristic peak at 30.16°, 35.53°, 43.18°, 53.57°, 57.11°, and 62.71°, which agrees well with reported done by Siregar et. al. (Siregar et al., 2020). All the observed diffraction peaks could be indexed by the cubic structure of Fe_3O_4 indicating a relative phase purity of iron oxide.

4.2 Photoluminescence

Figure 4.2a shows the PL emission of PbS QDs. It can be observed that the highest emission wavelength of PbS QDs is around 1631.42 nm. Moreels et al. (2009) reported that the wavelength corresponds to energy band gap of PbS was varying from 970 nm to 1740 nm (0.71 to 1.28 eV) depends on the size of the synthesized PbS QDs. Thus, we can confirm that the colloidal PbS QDs was successfully synthesized as they lie in this range.

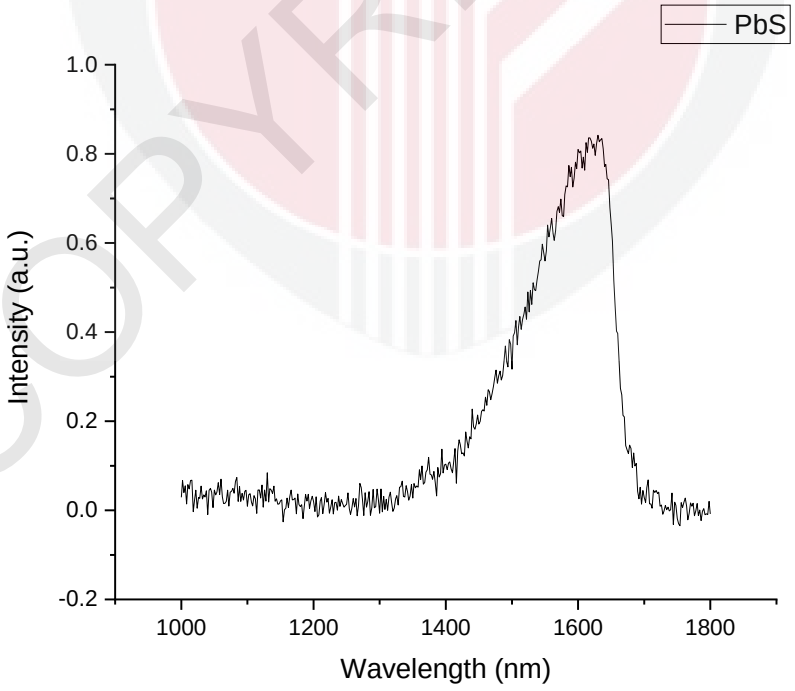

Figure 4.2a PL spectra of PbS QDs

The estimation size of PbS QDs size was obtained by using Brus equation (Chukwuocha et al., 2012)

$$\Delta E(R) = E_g(R) + \frac{h^2}{8R^2}(\frac{1}{m_e^*} + \frac{1}{m_h^*})$$

where $E(R)$ is the band-gap of the PbS in Joules, $E_g(R)$ is the bulk band-gap of PbS in Joules, and m_e^* and m_h^* are the effective masses of electrons and holes in PbS, respectively where m_e^* and m_h^* = 0.085m_0 and $m_0 = 9.11 \times 10^{-31}$ is the free-electron mass (Nanda et al., 2004). It was found that our colloidal PbS radius was 4.96 nm.

Figure 4.2b shows the PL intensity of PbS/Fe_3O_4 CSQDs with different volume of Fe_3O_4 between 0.2ml, 0.4ml and 0.6ml. PbS/Fe_3O_4 with the highest volume of Fe_3O_4 shows the highest PL peak intensity. This clearly indicated that luminescence of PbS/Fe_3O_4 CSQDs increases dramatically when we coated them with higher volume of Fe_3O_4 shell. The reason behind the increase in PL intensity is due to QDs surface modification (Zaini et al., 2020).

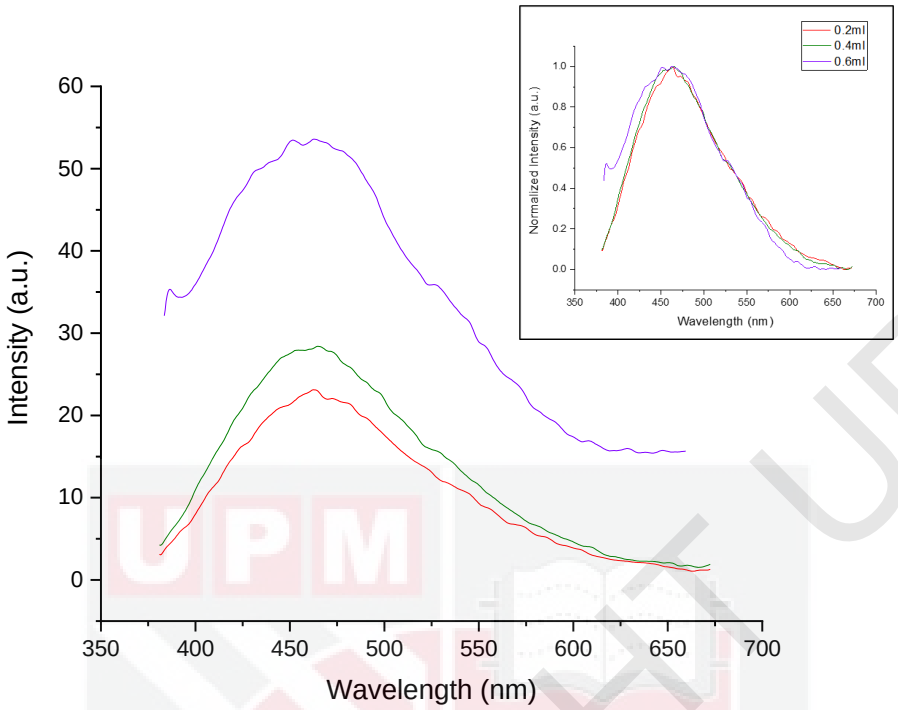

Figure 4.2b PL spectra of PbS/Fe_3O_4 CSQDs with different volume of Fe_3O_4

From the PL spectra presented in Figure 4.2b, we can see that the emission was blueshifted with increasing the volume of Fe_3O_4 between 0.2ml and 0.6ml. This anomalous optical properties is might due the role of cation/anion migration and/or exchange on compositional changes throughout the growth of CSQDs (Acebrón et al., 2018). The energy band diagram of the PbS/Fe_3O_4Y as depicted in Figure 4.2c.

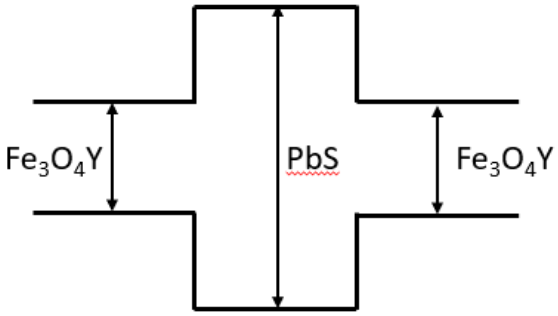

Figure 4.2c The energy band gap of CSQDs during migration or exchange of composition

Even though the cation/anion exchange might change the band gap, as we can observe, the band gap energy for Fe_3O_4 is still small and hence, all the recombination process of exciton still occurs in Fe_3O_4 shell. Thus, PbS/Fe3O4 still can be regard as type-I CSQDs.

4.3 UV-Vis Result

Figure 4.3 shows UV-Vis's spectra of PbS QDs and PbS/Fe3O4 CSQDs with different volume of Fe3O4.

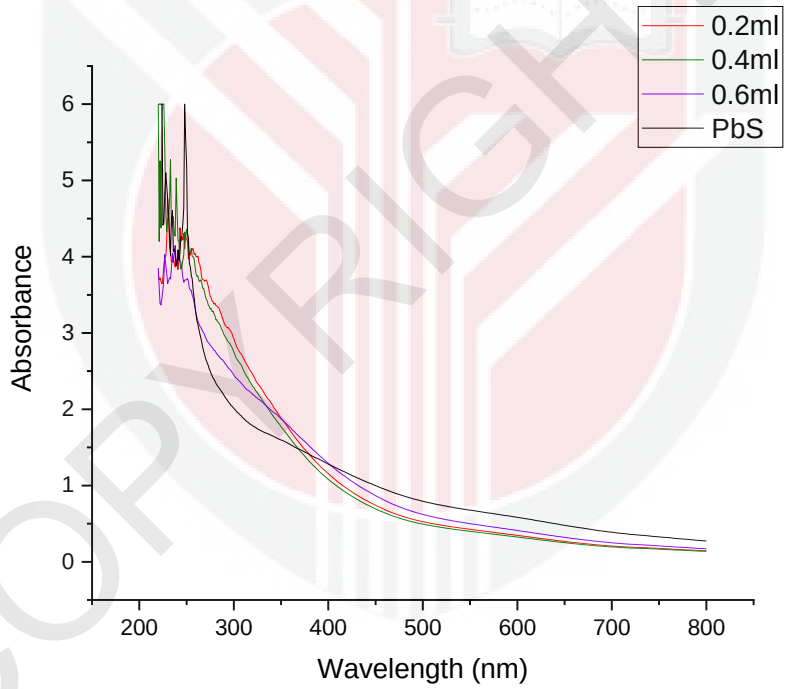

Figure 4.3 The UV-Vis spectra of PbS QDs and PbS/Fe_3O_4 CSQDs with different volume of Fe_3O_4

From the result of UV-Vis spectra, we can determine the energy band gap of the Fe_3O_4 shell by using Tauc plot method. The energy band gap will be state in the next section.

4.4 The Energy Band Gap of Fe_3O_4Y Shell

From PL spectra and UV-Vis, we can find the energy band gap of the Fe_3O_4Y shell. From Figure 4.2b, we can observe that as we increase the volume of Fe_3O_4, the graph is shifted towards lower wavelength i.e., blue shifted. The reason behind this is what being described from previous part where the blue shifted is due to the role of element migration and/or exchange on compositional changes throughout the growth of CSQDs (Acebrón et al., 2018). It means that as the volume of Fe_3O_4 is increasing, the migration process and the exchange of composition also increases. Hence, the blueshift also will increases.

The energy band gap of PbS/Fe_3O_4 for different volume of Fe_3O_4 is summarized in Table 4.4a below

Name of samples	Energy band gap, eV
PbS	0.77
PbS/Fe_3O_4 (0.2ml)	2.67
PbS/Fe_3O_4 (0.4ml)	2.68
PbS/Fe_3O_4 (0.6ml)	2.74

Table 4.4a The energy band gap of Fe_3O_4 with different volume of Fe_3O_4 shell from PL spectra

We can observe that the energy band gap is slightly increasing when the volume of Fe_3O_4 shell is increasing from 0.2ml to 0.4ml and then shows some greatly increasing when the volume of Fe_3O_4 is 0.6 ml. According to Ghandoor et al. (2012), the direct and indirect energy band gap of magnetite Fe_3O_4 sample is ranging from 0 to 3 eV depends on their size.

Next, we determine the energy band gap of Fe_3O_4 of different volume from UV-Vis result by using Tauc-plot method. The graph below shows UV-Vis's graph of PbS and PbS/Fe_3O_4 CSQDs after Tauc-plot method is applied.

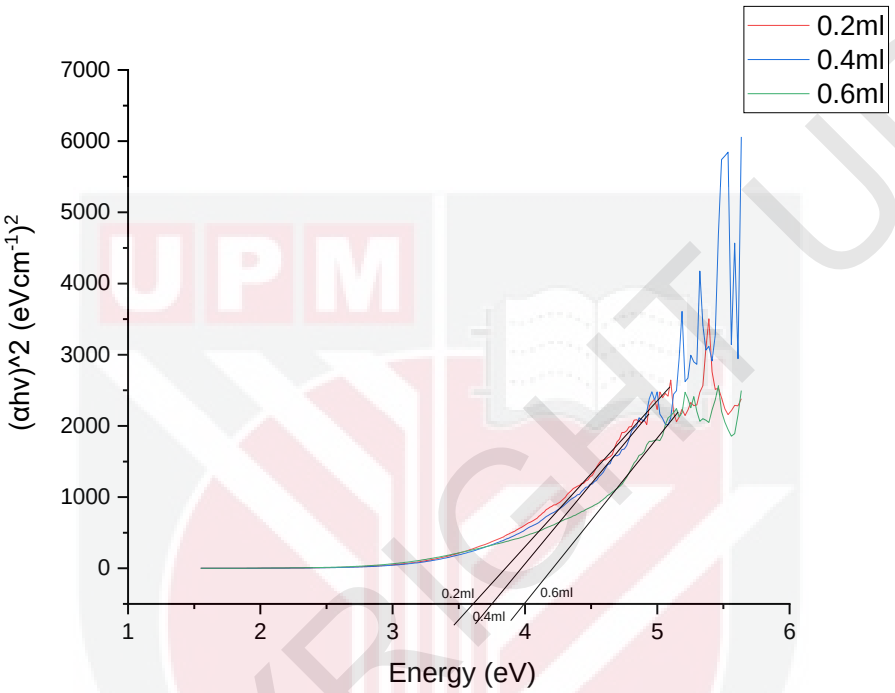

Figure 4.4a UV-Vis's graph of PbS/Fe_3O_4 CSQDs with different volume of Fe_3O_4 after Tauc plot method

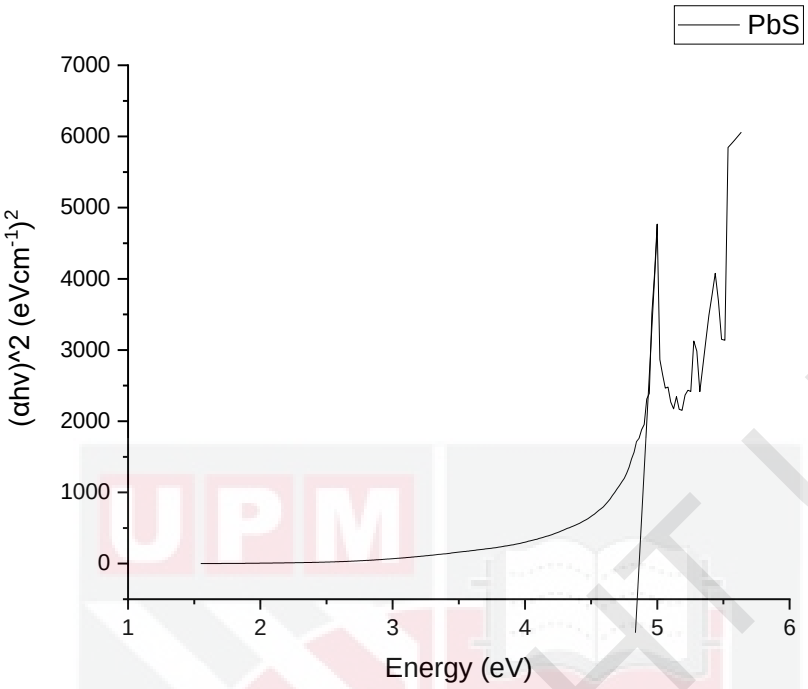

Figure 4.4b UV-Vis graph of PbS QDs after Tauc plot method

From Figure 4.4a and Figure 4.4b, we can determine the energy band gap of the PbS and Fe_3O_4 with different volume as shown in Table 4.4b

Name of samples	Energy band gap, eV
PbS	4.85
PbS/Fe_3O_4 (0.2ml)	3.61
PbS/Fe_3O_4 (0.4ml)	3.75
PbS/Fe_3O_4 (0.6ml)	4.0

Table 4.4b The energy band gap of Fe_3O_4 with different volume of Fe_3O_4 shell from UV-Vis spectra

From Table 4.4b, the trend of the energy band gap for different volume of Fe_3O_4 is same as PL spectra which is blue shifted. However, the energy band gap obtained from UV-Vis is not the same with PL spectra where the energy band gap from UV-Vis result is bigger than in PL spectra.

The reason behind this is because our sample experiencing a stoke shift. According to (Liu et al., 2018), Stokes shift is the shifting of spectral to lower energy between the incident light and the emitted light after interaction with a sample. For our sample, we can see that the emission energy from PL spectra is lower than the absorption energy from UV-Vis spectra. Hence, our samples clearly experience a Stoke shift.

4.5 Full Width Half Maximum (FWHM)

Figure 4.5 shows the graph of FWHM of PbS QDs and PbS/Fe3O4 CSQDs with different microwave volume of Fe3O4 shell from 0.2ml, 0.4ml, and 0.6ml.

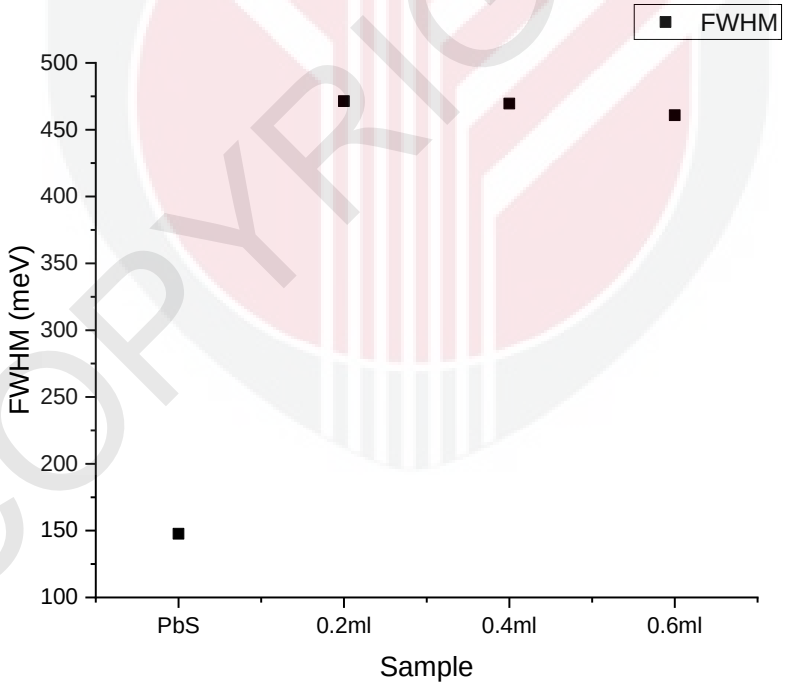

Figure 4.5 FWHM of PbS QDs and PbS/Fe_3O_4 CSQDs with different volume of Fe_3O_4

We can observe that the FWHM was increased from 147.66 to 471.32 meV and became narrower when growing Fe_3O_4 shell onto PbS core from 471.66, 469.52, and 460.88 meV for

volume of Fe_3O_4 equal to 0.2ml, 0.4ml, and 0.6ml, respectively. It was shown that by coating the PbS core with Fe_3O_4 shell, the size distribution of CSQDs becomes wider due to Fe_3O_4 shell becomes non homogeneous when coated with the PbS core (Vale et al., 2016). However, as the volume of Fe_3O_4 is increasing, the size of CSQDs becomes symmetrical and homogeneous (Jin et al., 2017).

CHAPTER 5

CONCLUSION

5.1 Conclusion

To conclude, we were able to synthesis colloidal PbS and PbS/Fe_3O_4 by using microwave synthesis method. The PbS QDs shows a near infrared emission at 1631.42 nm whereas the PbS/Fe_3O_4 shows a visible light emission at 450 – 470 nm for different volume of Fe_3O_4. Furthermore, we obtained a blueshift as we increase the volume of the shell. This blueshift emission is due to the increase of exchange of composition as the amount of Fe_3O_4 present in the solution during the mixture of PbS and Fe_3O_4 is increasing. Apart from that, we were able to obtained a high luminescence intensity when we coated the PbS quantum dots with Fe_3O_4 shell layer. Moreover, according to FWHM, the size distribution becomes unsymmetric when we coat the PbS core with the compound of Fe_3O_4 shell and then it tends to becomes symmetric and homogeneous as the volume of Fe_3O_4 increases to coat the PbS core. Apart from that, the synthesized PbS/Fe_3O_4 by microwave-assisted method also experience a stoke shifts where a redshift of an emission spectrum occurred with respect to the its absorption. Lastly, we can conclude that the PbS/Fe_3O_4 is not suitable for being used in vivo imaging because its emission does not appear in desired NIR window emission.

5.2 Recommendations for Future Research

This study might benefit from a number of further research suggestions. To begin, a PL spectrum for Fe_3O_4 that has not coated the PbS core can be obtained. By comparing the PL data of Fe_3O_4 and PbS/Fe_3O_4 CSQDs, we can examine any distinct homogeneous nucleation of Fe_3O_4 QDs. By doing so, we may determine if the volume of Fe_3O_4 required to cover the PbS core is insufficient, sufficient, or excessive. Furthermore, we can determine if the PL emission is caused by bulk Fe_3O_4.

Second, XRD examination of PbS with and without Fe_3O_4 shell may be done. The phase variations indicated by the distinctive peaks are used to validate the creation of the Fe_3O_4 shell surrounding the PbS core. The creation of Fe_3O_4 shell may be proven if the distinctive peaks of PbS/Fe_3O_4 CSQDs shift from PbS to Fe_3O_4 -like patterns.

Third, to elucidate the compositional changes throughout the synthesis of PbS/Fe_3O_4 CQDs, further characterizations such as X-Ray Photoelectron Spectroscopy (XPS), X-Ray Absorption Spectroscopy (XAS), and Total Reflection X-Ray Fluorescence (TXRF) may be performed. All of the characterization requires us to look for the existence of a compound in the shell, so we can determine the compound Y formed with Fe_3O_4 in the shell.

Finally, we can modify the PbS core molar ratio to alter the research parameter. The present molar ratio of Pb and S is 1: 0.56. So, other researchers can change this molar ratio to examine the influence of molar ratio on compositional changes and PL spectra.

REFERENCES

Acebrón, M., Galisteo-López, J. F., López, C., Herrera, F. C., Mizrahi, M., Requejo, F. G., Palomares, F. J., & Juárez, B. H. (2018). Unexpected Optical Blue Shift in Large Colloidal Quantum Dots by Anionic Migration and Exchange. *Journal of Physical Chemistry Letters*, *9*(11), 3124–3130. https://doi.org/10.1021/acs.jpclett.8b00741

Alizadeh-Ghodsi, M., Pourhassan-Moghaddam, M., Zavari-Nematabad, A., Walker, B., Annabi, N., & Akbarzadeh, A. (2019). State-of-the-Art and Trends in Synthesis, Properties, and Application of Quantum Dots-Based Nanomaterials. *Particle and Particle Systems Characterization*, *36*(2). https://doi.org/10.1002/ppsc.201800302

Bajwa, N., Mehra, N. K., Jain, K., & Jain, N. K. (2016). Pharmaceutical and biomedical applications of quantum dots. *Artificial Cells, Nanomedicine and Biotechnology*, *44*(3), 758–768. https://doi.org/10.3109/21691401.2015.1052468

Ballou, B., Lagerholm, B. C., Ernst, L. A., Bruchez, M. P., & Waggoner, A. S. (2004). *Noninvasive Imaging of Quantum Dots in Mice*. 79–86.

Battaglia, D., Li, J. J., & Wang, Y. (2003). *Colloidal Two-Dimensional Systems: CdSe Quantum Shells and Wells***. 5035–5039. https://doi.org/10.1002/anie.200352120

Bierwagen, O. (2015). Indium oxide — a transparent , wide-band gap semiconductor for (opto) electronic applications. *Semiconductor Science and Technology*, *30*(2), 24001. https://doi.org/10.1088/0268-1242/30/2/024001

Cademartiri, L., Bertolotti, J., Sapienza, R., Wiersma, D. S., Freymann, G. Von, & Ozin, G. A. (2006). *Multigram Scale, Solventless, and Diffusion-Controlled Route to Highly Monodisperse PbS Nanocrystals*. 671–673.

Chuang, C. H., Lo, S. S., Scholes, G. D., & Burda, C. (2010). Charge separation and recombination in CdTe/CdSe core/shell nanocrystals as a function of shell coverage: Probing the onset of the quasi type-II regime. *Journal of Physical Chemistry Letters*, *1*(17), 2530–2535. https://doi.org/10.1021/jz1008399

Chukwuocha, E. O., Onyeaju, M. C., & Harry, T. S. T. (2012). Theoretical Studies on the Effect of Confinement on Quantum Dots Using the Brus Equation. *World Journal of Condensed Matter Physics*, *02*(02), 96–100. https://doi.org/10.4236/wjcmp.2012.22017

Cui, H., Liu, Y., & Ren, W. (2013). Structure switch between α-Fe2O3, γ-Fe2O3 and Fe3O4 during the large scale and low temperature sol-gel synthesis of nearly monodispersed iron oxide nanoparticles. *Advanced Powder Technology*, *24*(1), 93–97. https://doi.org/10.1016/j.apt.2012.03.001

Da, L. E. I., Yongtao, S., Yiyu, F., & Wei, F. (2012). *Recent progress in the fields of tuning the band gap of*. *55*(4), 903–912. https://doi.org/10.1007/s11431-011-4717-1

Ezekoye, T, M. E., V, A. E., K, O. I., & P, O. O. (2015). Optical and structural properties of lead sulphide (PbS) thin films synthesized by chemical method. *International Journal of Physical Sciences*, *10*(13), 385–390. https://doi.org/10.5897/ijps2015.4354

Gil, H. M., Price, T. W., Chelani, K., Bouillard, J. S. G., Calaminus, S. D. J., & Stasiuk, G. J. (2021). NIR-quantum dots in biomedical imaging and their future. *IScience*, *24*(3). https://doi.org/10.1016/j.isci.2021.102189

Gravier, J., Navarro, F. P., Commission, A. E., Texier, I., & Commission, A. E. (2012). *Fluorescent Nanoprobes Dedicated to in Vivo Imaging: From Preclinical Validations to Clinical Translation*. *December*. https://doi.org/10.3390/molecules17055564

Hines, M. A., & Scholes, G. D. (2003). Colloidal PbS Nanocrystals with Size-Tunable Near-Infrared Emission: Observation of Post-Synthesis Self-Narrowing of the Particle Size Distribution. *Advanced Materials*, *15*(21), 1844–1849. https://doi.org/10.1002/adma.200305395

Huang, Z., Zhai, G., Zhang, Z., Zhang, C., Xia, Y., Lian, L., Fu, X., Zhang, D., & Zhang, J. (2017). Low cost and large scale synthesis of PbS quantum dots with hybrid surface passivation. *CrystEngComm*, *19*(6), 946–951. https://doi.org/10.1039/C6CE02471H

Jiang, W., Singhal, A., Zheng, J., Wang, C., & Chan, W. C. W. (2006). Optimizing the synthesis of red- to near-IR-emitting CdS-capped CdTe xSe1-x alloyed quantum dots for biomedical imaging. *Chemistry of Materials*, *18*(20), 4845–4854. https://doi.org/10.1021/cm061311x

Jin, S., Hu, Y., Gu, Z., Liu, L., & Wu, H. C. (2011). Application of quantum dots in biological imaging. *Journal of Nanomaterials*, *2011*. https://doi.org/10.1155/2011/834139

Jin, X., Bai, J., Gu, X., Chang, C., Shen, H., Zhang, Q., Li, F., Chen, Z., & Li, Q. (2017). Efficient light-emitting diodes based on reverse type-I quantum dots. *Optical Materials Express*, *7*(12), 4395. https://doi.org/10.1364/ome.7.004395

Kalantari, K., Ahmad, M. B., Shameli, K., Hussein, M. Z. Bin, Khandanlou, R., & Khanehzaei, H. (2014). Size-controlled synthesis of Fe3O4 magnetic nanoparticles in the layers of montmorillonite. *Journal of Nanomaterials*, *2014*. https://doi.org/10.1155/2014/739485

Kapatkar, P. S., Shettar, R. B., Kapatkar, S. B., & Patil2, N. R. (2018). *Synthesis , Structural and Optical Investigation of CdSe semiconductor Quantum Dots*. https://doi.org/10.1088/1757-899X/360/1/012009

Khalil, M. I. (2015). Co-precipitation in aqueous solution synthesis of magnetite nanoparticles using iron (III) salts as precursors. *Arabian Journal of Chemistry*, *8*(2), 279–284.

https://doi.org/10.1016/j.arabjc.2015.02.008

Lei, W., Liu, Y., Si, X., Xu, J., Du, W., Yang, J., Zhou, T., & Lin, J. (2017). Synthesis and magnetic properties of octahedral Fe3O4 via a one-pot hydrothermal route. *Physics Letters, Section A: General, Atomic and Solid State Physics*, *381*(4), 314–318. https://doi.org/10.1016/j.physleta.2016.09.018

Li, L., Daou, T. J., Texier, I., Chi, T. T. K., Liem, N. Q., & Reiss, P. (2009). Highly luminescent cuins 2/ZnS Core/Shell nanocrystals: Cadmium-free quantum dots for in vivo imaging. *Chemistry of Materials*, *21*(12), 2422–2429. https://doi.org/10.1021/cm900103b

Liu, D., Lei, W., Qin, S., Hou, L., Liu, Z., Cui, Q., & Chen, Y. (2013). *Large-scale synthesis of hexagonal corundum-type In2O3 by ball milling with enhanced lithium storage capabilities*. *c*, 5274–5278. https://doi.org/10.1039/c3ta00182b

Liu, Y., Kim, D., Morris, O. P., Zhitomirsky, D., & Grossman, J. C. (2018). Origins of the Stokes Shift in PbS Quantum Dots: Impact of Polydispersity, Ligands, and Defects. *ACS Nano*, *12*(3), 2838–2845. https://doi.org/10.1021/acsnano.8b00132

Mansur, H. S., Mansur, A. A. P., & González, J. C. (2011). Synthesis and characterization of CdS quantum dots with carboxylic- functionalized poly (vinyl alcohol) for bioconjugation. *Polymer*, *52*(4), 1045–1054. https://doi.org/10.1016/j.polymer.2011.01.004

Manzoor, U., Islam, M., Tabassam, L., & Rahman, S. U. (2009). Quantum confinement effect in ZnO nanoparticles synthesized by co-precipitate method. *Physica E: Low-Dimensional Systems and Nanostructures*, *41*(9), 1669–1672. https://doi.org/10.1016/j.physe.2009.05.016

Martinez, A. I., Garcia-Lobato, M. A., & Perry, D. L. (2015). Study of the properties of iron oxide nanostructures. *New Nanotechnology Developments*, *January*, 183–194.

Moreels, I., Lambert, K., Smeets, D., & De Muynck, D. (2009). Size-Dependent Optical Properties of Colloidal PbS Quantum Dots - ACS Nano (ACS Publications). *Acs Nano*, *3*(10), 3023–3030. http://pubs.acs.org/doi/abs/10.1021/nn900863a

Mozafari, M., & Moztarzadeh, F. (2010). Controllable synthesis, characterization and optical properties of colloidal PbS/gelatin core-shell nanocrystals. *Journal of Colloid and Interface Science*, *351*(2), 442–448. https://doi.org/10.1016/j.jcis.2010.08.030

Nanda, K. K., Kruis, F. E., Fissan, H., Behera, S. N., Nanda, K. K., Kruis, F. E., & Fissan, H. (2004). *Effective mass approximation for two extreme semiconductors : Band gap of PbS and CuBr nanoparticles Effective mass approximation for two extreme semiconductors : Band gap of PbS and CuBr nanoparticles*. *5035*(May 2013). https://doi.org/10.1063/1.1691184

Qutub, N., & Sabir, S. (2012). Optical, Thermal and Structural Properties of CdS Quantum Dots Synthesized by A Simple Chemical Route. *International Journal of Nanoscience and Nanotechnology*, *8*(2), 111–120.

Parkinson, G. S. (2016). Iron oxide surfaces. *Surface Science Reports*, *71*(1), 272–365. https://doi.org/10.1016/j.surfrep.2016.02.001

Patsula, V., Moskvin, M., Dutz, S., & Horák, D. (2016). Size-dependent magnetic properties of iron oxide nanoparticles. *Journal of Physics and Chemistry of Solids*, *88*, 24–30. https://doi.org/10.1016/j.jpcs.2015.09.008

Paul Pistor, A., *‡ Jose M. Merino A´ lvarez, b Ma´ximo Leo´n, b Marco di Michiel, c S., & Schorr, a, d R. K. and S. L. (2016). *Structure reinvestigation of a - , b - and c -In 2 S 3 research papers*. 410–415. https://doi.org/10.1107/S2052520616007058

Reiss, P., Protière, M., & Li, L. (2009). Core/shell semiconductor nanocrystals. *Small*, *5*(2), 154–168. https://doi.org/10.1002/smll.200800841

Román-Zamorano, J. F., Flores-Acosta, M., Arizpe-Chávez, H., Castillón-Barraza, F. F., Farías, M. H., & Ramírez-Bon, R. (2009). Structure and properties of lead and lead sulfide nanoparticles in natural zeolite. *Journal of Materials Science*, *44*(18), 4781–4788. https://doi.org/10.1007/s10853-009-3720-4

Sadovnikov, S. I., Gusev, A. I., & Rempel, A. A. (2016). Nanostructured lead sulfide: synthesis, structure and properties. *Russian Chemical Reviews*, *85*(7), 731–758. https://doi.org/10.1070/rcr4594

Shariati, M. R., Samadi-Maybodi, A., & Colagar, A. H. (2018). Dual cocatalyst loaded reverse type-I core/shell quantum dots for photocatalytic antibacterial applications. *Journal of Materials Chemistry A*, *6*(41), 20433–20443. https://doi.org/10.1039/c8ta07583b

Siregar, J., Sebayang, K., & Yuliarto, B. (2020). *XRD characterization of Fe 3 O 4 -ZnO nanocomposite material by the hydrothermal method XRD Characterization of Fe 3 O 4 - ZnO Nanocomposite Material by the Hydrothermal Method*. *110008*(March), 6–10.

Smith, A. M., & Nie, S. (2010). Semiconductor nanocrystals: Structure, properties, and band gap engineering. *Accounts of Chemical Research*, *43*(2), 190–200. https://doi.org/10.1021/ar9001069

Smyder, J. A., & Krauss, T. D. (2011). Coming attractions for semiconductor quantum dots. *Materials Today*, *14*(9), 382–387. https://doi.org/10.1016/S1369-7021(11)70182-1

Stephen, Z. R., Kievit, F. M., & Zhang, M. (2011). Magnetite Nanoparticles for Medical MR Imaging. *Bone*, *23*(1), 1–7. https://doi.org/10.1016/S1369-7021(11)70163-8.Magnetite

Subila, K. B., Kumar, G. K., Shivaprasad, S. M., & Thomas, K. G. (2013). *Luminescence Properties of CdSe Quantum Dots: Role of Crystal Structure and Surface Composition*.

Sun, Z., Kumbhar, A., Sun, K., Liu, Q., & Fang, J. (2008). One-pot synthesis of reverse type-I In2O3@In 2S3 core-shell nanoparticles. *Chemical Communications*, *16*, 1920–1922. https://doi.org/10.1039/b719176f

Tian, Y., Wu, D., Jia, X., Yu, B., & Zhan, S. (2011). *Core-Shell Nanostructure of α -Fe2O3 / Fe3O4 : Synthesis and Photocatalysis for Core-Shell Nanostructure of α -Fe 2 O 3 / Fe 3 O 4 : Synthesis and Photocatalysis for Methyl Orange*. *January*. https://doi.org/10.1155/2011/837123

Uzar, N., & Arikan, M. C. (2011). Synthesis and investigation of optical properties of ZnS nanostructures. *Bulletin of Materials Science*, *34*(2), 287–292. https://doi.org/10.1007/s12034-011-0085-5

Wang, D., Zhang, X., Li, B., Liu, L., & Shen, D. Z. (2015). *Dynamical properties and their strain-dependence of ZnSe (ZnSe : N): Zinc-blende and wurtzite*. *067138*(April 2014). https://doi.org/10.1063/1.4885466

Xu, M., Li, Y., Yao, B., Ding, Z., & Yang, G. (2014). Structural , electronic and optical properties of Cd x Zn 1 − x S alloys from first-principles calculations. *Physics Letters A*, *378*(45), 3382–3388. https://doi.org/10.1016/j.physleta.2014.09.036

YIN, S. (2018). *YIN, SHICHEN. Achieving High-Performance Infrared Range (IR) Photodiode via Bilayer Lead Sulfide Quantum Dots (QDs) Structure*.

Zaini, M. S., Ying, J., Liew, C., Ainliah, S., Ahmad, A., Mohmad, A. R., & Kamarudin, M. A. (2020). applied sciences Quantum Confinement E ff ect and Photoenhancement of Photoluminescence of PbS and PbS / MnS Quantum Dots. *Applied Sciences*, *10*(6282), 1–10.

Zhang, J., Gao, J., Miller, E. M., Luther, J. M., & Beard, M. C. (2014). Diffusion-controlled synthesis of PbS and PbSe quantum dots with in situ halide passivation for quantum dot solar cells. *ACS Nano*, *8*(1), 614–622. https://doi.org/10.1021/nn405236k

Zhong, X., Xie, R., Zhang, Y., Basché, T., & Knoll, W. (2005). High-quality violet- To red-emitting ZnSe/CdSe core/shell nanocrystals. *Chemistry of Materials*, *17*(16), 4038–4042. https://doi.org/10.1021/cm050948y

Zia, M., Phull, A. R., & Ali, J. S. (2016). Synthesis, characterization, applications, and challenges of iron oxide nanoparticles. *Powder Technology*, *7*(6), 49–67.

APPENDICES

1. Calculation Of Estimated Monolayer (ML) Of Shell

$$\text{Volume of PbS core} = \frac{4}{3}\pi\ (4\ nm\ )^3 = 268.08\ \text{nm}^3$$

$$\text{Volume of one-unit cubic PbS} = (0.594\ nm)^3 = 0.209\ \text{nm}^3$$

1 unit of cubic = 0.209 nm^3

If $268.08\ \text{nm}^3$, so

$$\text{unit of cubic} = \frac{268.08\ \text{nm}^3}{0.209\ \text{nm}^3} = 1283\ \text{unit of PbS}$$

PbS is Face center cubic (has 4 atom), so in one unit cell (4 Pb + 4 S)

Atom = 1283 unit of PbS x 8 atom = 10264 atoms of PbS in 1 QDs

∴ 1 QDs have 10264 atoms of PbS

In 5 ml PbS (5 ml Pb + 0.245 ml S)

Pb,

$$\text{Number of Mol} = \frac{MV}{1000} = \frac{0.0166\text{x } 5\ \text{ml}}{1000} = 0.000083\ \text{mol}$$

Atom = mol x Avogadro constant =0.000083 mol x ($6.02 \times 10^{23}\ \text{mol}^{-1}$) =4.9966 x 10^{19}

S,

$$\text{Number of Mol} = \frac{MV}{1000} = \frac{0.1\text{x } 0.245\ \text{ml}}{1000} = 2.45 \text{ x } 10^{-5}\ \text{mol}$$

Atom = mol x Avogadro constant =2.45 x 10^{-5} mol x ($6.02 \times 10^{23}\ \text{mol}^{-1}$) = 1.47 x 10^{19}

Total PbS in 5 ml,

Pb +S =4.9966 x 10^{19} + 1.47 x 10^{19} = 6.47 x 10^{19}

S x 2= 1.47 x 10^{19} x 2 = 2.94 x 10^{19} (assume all S is used)

∴ Pb has 2.94 x 10^{19} atom in 5 ml solution

We know 1 QDs have 10264 atoms of PbS

If 2.94 x 10^{19} atom of Pb, we have

$$\frac{1}{10264\ \text{atom}} \text{ x } 2.94 \text{ x } 10^{19} \text{ atom} = 2.86 \text{ x } 10^{15} \text{ PbS QDs}$$

$$\text{Mol of } Fe_3O_4 = \frac{\text{molarity} \times \text{volume}}{1000} = \frac{0.1\ \text{M} \times 0.1\ \text{ml}}{1000} = 0.00001 \text{ mol}$$

Atom = mol x Avogadro constant = 0.00001 mol x ($6.02 \times 10^{23}\ \text{mol}^{-1}$) = $\underline{6.02 \times 10^{18} \text{ atom}}$

∴ 0.1 ml Fe_3O_4 have 6.02×10^{18} atom

1 monolayer = 0.84 nm

If 1 ML,

$$\text{Volume of shell+ core} = \frac{4}{3}\pi\ (4\ nm + 0.84\ nm)^3 = 475\ \text{nm}^3$$

Volume of shell = (Volume of shell+ core)- (Volume of PbS core)

$$= 475\ \text{nm}^3 - 268.08\ \text{nm}^3$$

$$= 207\ \text{nm}^3$$

1 unit of cubic = 0.84 nm^3

If 207 nm^3, so

$$\text{unit cell of } Fe_3O_4 \text{ is } \frac{207\ nm^3}{0.84\ nm^3} = 246 \text{ unit}$$

Fe_3O_4 is

face center cubic with 8 lattice point =246(8) = 1968 atom

Atom need to grow shell =2.86 x 10^{15} PbS QDs x (1968 atom of Fe_3O_4)

=5.64 x 10^{18} atom of Fe_3O_4 needed for 1ML

i.e., 5.64 x 10^{18} atom Fe_3O_4 = 1 ML

If 6.02×10^{18} atom, we get

$$\frac{1}{5.64 \text{ x } 10^{18}} \text{x } 6.02 \times 10^{18} = 1.07 \text{ ML}$$

∴ 1.07 ML or 0.90 nm is the thickness of shell.

2. Calculation of PbS core size

$$\Delta E(R) = E_g(R) + \frac{h^2}{8R^2}\left(\frac{1}{m_e^*} + \frac{1}{m_h^*}\right)$$

Where

$$\Delta E(R) = Energy\ band\ gap\ of\ PbS = 0.77\ eV = 1.234 \times 10^{-19}\ J$$

$$E_g(R) = Energy\ band\ gap\ of\ bulk\ PbS = 0.41\ eV = 0.6569 \times 10^{-19}\ J$$

$$m_e^* = m_h^* = 0.085 m_0 = 0.085(9.11 \times 10^{-31}) = 7.7435 \times 10^{-32}$$

So, the radius of PbS is

$$1.234 \times 10^{-19} = 0.6569 \times 10^{-19} + \frac{h^2}{8R^2}\left(\frac{1}{7.7435 \times 10^{-32}} + \frac{1}{7.7435 \times 10^{-32}}\right)$$

$$R = 4.956\ nm$$

Hence its diameter size is

$$d = 9.91\ nm$$